ISSN 0020-4412, Instruments and Experimental Techniques, 2015, Vol. 58, No. 5, pp. 711–717. © Pleiades Publishing, Ltd., 2015.
Original Russian Text © I.I. Maslenikov, V.N. Reshetov, A.S. Useinov, 2015, published in Pribory i Tekhnika Eksperimenta, 2015, No. 5, pp. 136–142.

LABORATORY TECHNIQUES

Mapping the Elastic Modulus of a Surface with a NanoScan 3D Scanning Microscope

I. I. Maslenikov[a]*, V. N. Reshetov[b], and A. S. Useinov[c]

[a]*Moscow Institute of Physics and Technology, Institutskii per. 9, Dolgoprudnyi, Moscow oblast, 141700 Russia*
[b]*National Research Nuclear University MEPhI, Kashirskoe sh. 31, Moscow, 115409 Russia*
[c]*FGBNU TISNUM, ul. Tsentral'naya 7a, Troitsk, Moscow, 142190 Russia*
**e-mail: igor.maslenicov@gmail.com*

Received August 27, 2014; in final form, October 29, 2014

Abstract—The possibility of mapping the elasticity modulus during scanning of the material surface with a piezoresonance probe is proposed. An analytical model is proposed that describes the force of an elastic interaction between the surface and an indenter in the form of a truncated cone as a function of a displacement. Within the framework of this model, dependences were obtained that allow the elasticity-modulus value to be determined, provided that the data on the average force of a semicontact interaction, the amplitude, and the frequency of probe resonance oscillations are available. The obtained dependences were used for mapping the elasticity modulus of the boundaries of deposited aluminum and copper films on glass, as well as for a TGZ2 test structure. Experiments were performed using a NanoScan 3D scanning nanohardness tester, and a resolution of 0.2 μm was attained. This technique is applicable to materials that allow only an elastic deformation and can be used in instruments that can operate in a range of contact forces providing predominantly elastic deformations.

DOI: 10.1134/S0020441215040223

INTRODUCTION

Determining the mechanical properties at the nano- and microlevels is a constituent of the complex estimate of the quality of articles of different purposes [1, 2]. In some cases, the hardness or elasticity modulus is investigated using the methods for measuring the dependences of the corresponding quantities on spatial coordinates [3, 4]. In this case, the scanning-probe microscopy methods pretend to a nondestructive measurement of a local value of the elasticity modulus of an investigated nanostructured material.

The mapping of mechanical properties can be performed by using an approach in which a map of the surface hardness and elastcity modulus results from processing of an array of single measurements [3], which are carried out at different points of the sample surface using the instrumental-indentation method [5]. A method in which force signals and resonance-frequency-shift signals are recorded in the semicontact mode during scanning of a sample is used to obtain hardness maps [6]. The subsequent processing of the obtained data provides obtainment of the hardness map of the sample surface, if the elasticity modulus is known; if such a priori information is absent, the method allows mapping of the ratio of the hardness to the square of the elasticity modulus. Elasticity-modulus maps can be also obtained during the sample scanning process. The appropriate technique implies a continuous interaction of the indenter tip with a sample with maintenance of a constant pressing force on which a harmonic modulation is imposed. Information on the shift amplitude and phase at known values of the force amplitude and phase allows one to obtain information on the elasticity modulus [7]. Such methods imply that the probe–surface interaction is described by purely elastic forces and a plastic deformation of a material is absent; the value of the constant force component usually lies within a range of 1–100 μN.

Several elasticity-modulus measurement techniques, which were implemented by manufacturers of atomic-force microscopes (AFMs), also exist [2, 8–10]. To obtain the elasticity modulus during scanning, the pressing forces that are used in AFMs are substantially lower than those in scanning nanohardness testers. In the considered devices, the typical pressing forces range from 1 to 100 nN, thus determining the necessity of using models in which adhesion forces are considered. It is natural that the measured elasticity-modulus value depends in this case on the type of the chosen model [11]. This in turn requires additional a priori information on the object under study.

This study considers the possibility of mapping the elasticity modulus using a piezoresonace probe, which is used in a NanoScan 3D scanning nanohardness tester. This instrument is able to operate in both the scan-

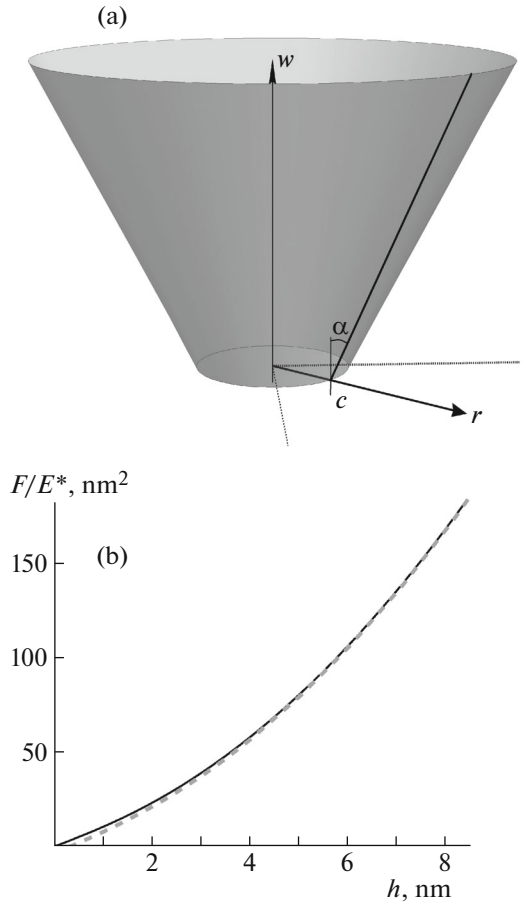

Fig. 1. (a) The indenter-shape-approximating model constructed according to (5); (b) model dependences of the ratio of the pressing force to the elasticity modulus on the indentation depth of the indenter: (dashed curve) calculation using formula (13) and (solid curve) calculation using formulas (11) and (12).

ning-probe-microscope (SPM) and instrumental-indentation modes and was repeatedly described in the literature [12–15]. Let us briefly describe its operating principle.

The probe of the instrument has the form of a tuning fork whose branches are piezoceramic bimorphs. A diamond indenter, which is attached to the free end of one branch, was brought into contact with the material surface during measurements. In the scanning mode and, if necessary, in the indentation mode, a signal is fed from the self-excited-oscillator channel to one of the branches. A signal that is picked off the other branch arrives at the input of the self-excited-oscillator channel. The tuning-fork branches are attached to the central leg whose bending stiffness is low (a probe with a stiffness of 0.4 kN/m was used in this study). A bend of the leg during a contact of the probe with the surface is detected by an optical detector and converted into a force signal. In the SPM mode, when a constant resonance-frequency shift is maintained, the probe is able to scan the surface relief.

DESCRIPTION OF THE MATHEMATICAL MODEL

The proposed method is based on the dependences that determine the interrelations between the shift of the resonance frequency ω_0 of probe oscillations and the amplitude and force of the indenter interaction with the surface. This approach was first demonstrated in [16], and analogous equations were obtained by another method in [17], from which it follows that

$$\frac{\omega^2}{\omega_0^2} - 1 = \frac{1}{\pi}\int_0^{2\pi} \frac{F\left(h\left(\frac{\tau}{\omega}\right)\right)}{kA} \frac{z\left(\frac{\tau}{\omega}\right)}{A} d\tau, \quad (1)$$

where k is the dynamic rigidity and A is the amplitude of probe oscillations that follow a harmonic law:

$$z(t) = z_0 - A\cos(\omega t); \quad (2)$$

$h(t)$ is the depth of the indenter penetration into the surface:

$$h(t) = \begin{cases} 0, & z(t) > 0 \\ -z(t), & z(t) \le 0; \end{cases} \quad (3)$$

$F(t)$ is the indenter–sample interaction force.

In view of the fact that during an elastic interaction, the force depends on the substance elasticity modulus, Eq. (1) can be used for mapping this quantity. However, according to (1), for this purpose, it is necessary to know the current position z_0 of the probe. It is natural that when a heterogeneous sample is scanned, this value changes, and determining the elasticity modulus requires additional information, e.g., on the average value of the pressing force of the tip applied to the surface. In NanoScan instruments, the force F_a of the probe interaction with the surface, which is averaged over a period, is recorded. In the case of measuring the instantaneous force value several times in an oscillation period and using the proposed method, the obtained values should be averaged. The average force F_a is defined as

$$F_a = \frac{1}{2\pi}\int_0^{2\pi} F\left(h\left(\frac{\tau}{\omega}\right)\right) d\tau. \quad (4)$$

To determine the contact force $F(h)$, let us consider an elastic interaction of the indenter with the surface. When the shape of the indenter tip is described by a paraboloid of revolution, the corresponding dependence of the force on the indentation depth is described by the Hertz formula [18]. On the other hand, to take the indenter-tip blunting (which is characterized by the quantity Δh) an approximation corresponding to a truncated pyramid is used [19, 20], for which the dependence of the area on the height is

expressed by the formula $A = 24.5(h + \Delta h)^2$. Without taking the pyramid asymmetry into account, this consideration is equivalent to the application of a model in which the indenter is represented as a truncated cone. The possibility of disregarding the asymmetry is indicated by the fact that for the instrumental-indentation technique, the corresponding coefficient β, which introduces a multiplicative correction into the measured elasticity-modulus value, differs from unity quite negligibly [5]. It should be also noted that the height Δh, by which the model shape was "truncated," is only several nanometers [21], and at large indenter penetration depths into a sample, the indenter shape becomes close to pyramidal. In view of the fact that typical probe indentation depths in this study were >10 nm, it can be stated that in the case of an elastic interaction, the shape of a truncated cone is more correct than the shape of a paraboloid of revolution, for it allows consideration for the indenter imperfection and, at the same time, gives the correct asymptotics of the increase in the contact area as a function of the probe penetration into the sample: $A \sim h^2$.

DETERMINING THE FUNCTION FOR A TRUNCATED CONE

Let us consider that the indenter shape in a polar coordinate system can be described by the function

$$w(r) = \begin{cases} 0, & r < c \\ br - cb, & r \geq c. \end{cases} \quad (5)$$

In this case, $b = \cot\alpha$, where α is the angle between the height and generatrix of the truncated cone and c is the radius of the area that corresponds to the vertex of the truncated cone (Fig. 1a).

It was shown in [22] that for an indenter whose shape results from the rotation of an arbitrary function $w(r)$ around the vertical axis, the equations that specify the dependence of the force on the depth have the form:

$$F = 2E^* a \int_0^1 \frac{x^2 f'(x)}{\sqrt{1-x^2}} dx; \quad (6)$$

$$h = \int_0^1 \frac{f'(x)}{\sqrt{1-x^2}} dx, \quad (7)$$

where $f(x)$ is defined by the equation $f(r/a) = w(r)$. Symbol E^* denotes the reduced elasticity modulus, and a is the radius of the contact region. Original paper [22] considers the case of indentation of a perfectly rigid indenter into a surface; in this case, E^* and the Young modulus E of a material are interrelated through the formula $E^* = E/(1-\nu^2)$. Despite the fact that for a diamond indenter, a correction to a deformation that arises upon a contact with most materials is small, we take this effect into account by using

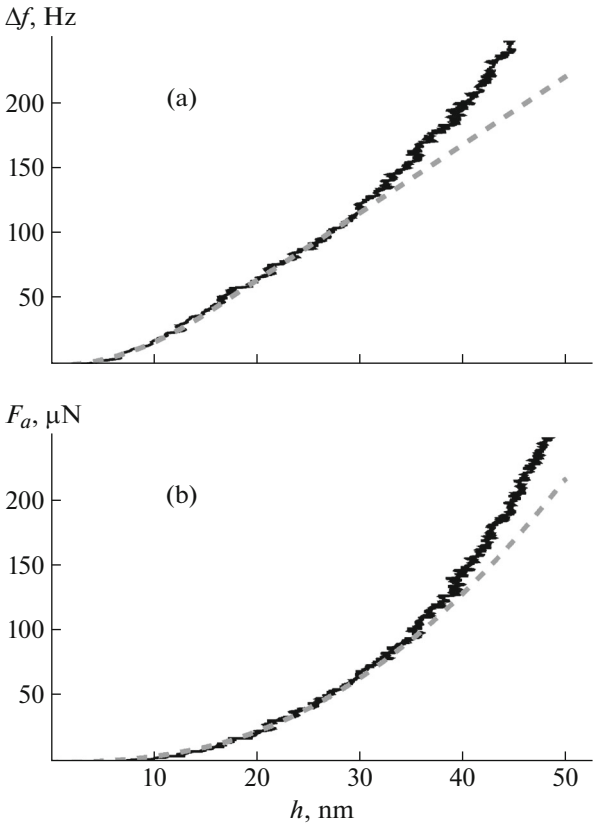

Fig. 2. Experimental (solid line) and model (dashed line) dependences of (a) the oscillation-frequency shift and (b) the force of pressing the indenter to the surface on the indentation depth.

the effective modulus E^*, which is defined by the equation [23]:

$$\frac{1}{E^*} = \frac{1-\nu^2}{E} + \frac{1-\nu_{ind}^2}{E_{ind}}, \quad (8)$$

where E_{ind} and ν_{ind} are, respectively, the Young modulus and the Poisson ratio for the indenter.

For the above-described function $f(x)$, these equations lead to the following result:

$$F = E^* b(c\sqrt{a^2 - c^2} + a^2 \arccos(c/a)); \quad (9)$$

$$h = ab\arccos(c/a). \quad (10)$$

The exact analytical expression for the dependence $F(h)$ cannot be found from this system, but a good approximation for a wide range of indentation depths (from a fraction of the c value and larger) can be obtained. For this purpose, we expand expressions (9) and (10) at small values of c/a. As is seen from Eq. (9), this situation corresponds to large values of h:

$$h(a) = \frac{b\pi a}{2} - bc - \frac{bc^3}{6a^2} + O\left(\frac{c}{a}\right)^4; \quad (11)$$

$$F(a) = E^*\left(\frac{\pi b a^2}{2} - \frac{2bc^3}{3a} - \frac{bc^5}{5a^3}\right) + O\left(\frac{c}{a}\right)^4. \quad (12)$$

Omitting higher-order terms, the following expression for the force can be obtained:

$$F(h) = E^*\frac{b^3c^3\pi^2 - 6(bc+h)^3}{3b(bc+h)\pi}. \quad (13)$$

Let us show that this expression for the force correctly describes the dependence $F(h)$ for typical values of the parameters b and c in the region of small depths. The value of the parameter b is determined by the cone vertex angle. For an ideal cone to have the same ratio between the height and the cross-sectional area as that for a Berkovich pyramid ($A = 24.5h^2$), its opening angle must be 70.32°. In view of the fact that at deep indentations, the asymptotic value of A/h^2 must be close to 24.5, and the value of b must also be close to cotan(70.32°).

In this experiment, the values $b = \cot(70°)$ and $c =$ 5 nm were used. The dependence exactly for such parameters is presented in Fig. 1b. The coincidence of the approximating solution corresponding to formula (13) (gray dashed curve) with the parametric dependence in accordance with formulas (11) and (12) (black solid curve) begins already with fractions of a nanometer.

Averaging according to formula (1) leads to the following result:

$$\frac{\omega^2}{\omega_0^2} - 1 = \frac{E^*}{Ak}\frac{2\tan\alpha}{3A\pi^2}\begin{cases} 0, & z_0 < A; \\ (c^3\pi^2\cot^3\alpha + 6A^2z_2)\arccos(z_0/A) & \\ -2(2A^2 + z_0^2 + 3z_2(z_2 - z_0))\sqrt{A^2 - z_0^2} & -A < z_0 < A; \\ +\dfrac{2c^3\pi^2\cot^3(\alpha)z_2}{\sqrt{A^2 - z_2^2}}\arctan\left(\dfrac{\sqrt{A - z_0}}{\sqrt{A + z_0}}\dfrac{\sqrt{A + z_2}}{\sqrt{A - z_2}}\right), & \\ \dfrac{\pi}{\sqrt{z_2^2 - A^2}}(c^3\pi^2\cot^3(\alpha)z_2 + (c^3\pi^2\cot^3\alpha & z_0 < -A, \\ +6A^2z_2)\sqrt{z_2^2 - A}), & \end{cases} \quad (14)$$

where

$$z_2 = z_0 - c\cot\alpha. \quad (15)$$

Calculating the average force from formula (4) leads to the expression

$$F_a = \frac{E^*\tan\alpha}{\pi^2}\begin{cases} 0, & z_0 < A; \\ (4z_2 - z_0)\sqrt{A^2 - z_0^2} - (A^2 + 2z_2^2)\arccos\left(\dfrac{z_0}{A}\right) & \\ -\dfrac{c^3\pi^2\cot^3\alpha}{3\sqrt{A^2 - z_2^2}}\ln\left(\dfrac{A(z_0 - z_2)}{A^2 - z_0z_2 + \sqrt{A^2 - z_0^2}\sqrt{A^2 - z_2^2}}\right), & -A < z_0 < A; \\ \pi\left(-\dfrac{c^3\pi^2\cot^3(\alpha)}{3\sqrt{z_2^2 - A^2}} - (A^2 + 2z_2^2)\right), & z_0 < -A. \end{cases} \quad (16)$$

Equations (14) and (16) specify the system of equations

$$\begin{cases} F_a = F_a(E^*, A, z_0) \\ \omega = \omega(E^*, A, z_0) \end{cases} \quad (17)$$

and at predetermined values of the force F_a, amplitude A and frequency ω, they can be solved with respect to the reduced modulus E^* and the average value of the probe position z_0.

Thus, by measuring the resonance-frequency shift $\Delta f = \dfrac{\omega - \omega_0}{2\pi}$ during scanning, the force F_a, and the amplitude A, one can construct a map of the elasticity modulus $\dfrac{E}{1 - \nu^2}$ of a sample. As additional quantities, information on the parameters ω_0, c, α, k, E_{ind}, and ν_{ind} is required. The value of the free-probe resonance frequency ω_0 is measured, and the parameters E_{ind} and ν_{ind} are usually known, as well as the indenter material. The value of the parameter α is determined by the

dependence of the projection of the contact area on the depth for the used indenter. To determine the values of the parameters c and k, the "bringing curves" are used (dependences of the force and resonance-frequency shift on the probe indentation depth into a sample, Fig. 2). These curves are approximated by the theoretical dependences, according to formulas (17), at different values of these parameters. The initial value of the dynamic rigidity k_0 for seeking the actual value of k can be estimated as $k_0 \approx \omega_0 m^2$, where m is the mass of the movable part of the oscillating element. As was mentioned above in the description of the mathematical model, the value of Δh, by which the cone is truncated, is usually several nanometers; therefore, the initial value of $c_0 = \Delta h \tan\alpha$ is $\leqslant 10$ nm. The correct choice of c and k must provide the coincidence of the initial segments of the indenter bringing (IB) curves that were measured at different amplitudes.

To obtain the calibration IB curves, fused silica was chosen as the material that is commonly used to calibrate nanoindenters. Typical dependences of the frequency shift Δf and the force F_a on the indentation depth h in the sample are shown in Fig. 2; in the measurements of these curves, the oscillation amplitude was 10 nm. The parameter b was chosen equal to cot70°: this value provides the required asymptotics of the area as a function of the depth for a pyramid whose area is close to an ideal one. The parameters c and k, which provide the coincidence of the calculated and experimental dependences, occurred to be equal to 5 nm and 3.5×10^6 N/m, respectively. Synthetic diamond (E = 1140 GPa, ν = 0.07), was used as the indenter at $\omega_0 = 92 \times 10^3$ rad/s.

According to Fig. 2, the model dependences coincide with the experimental data to an indentation depth of ~30 nm. This is a rather large indentation, and all the data presented below were obtained at smaller resonance-frequency shifts, forces, and indentation depths, i.e., in the region where the model and experimental curves coincide.

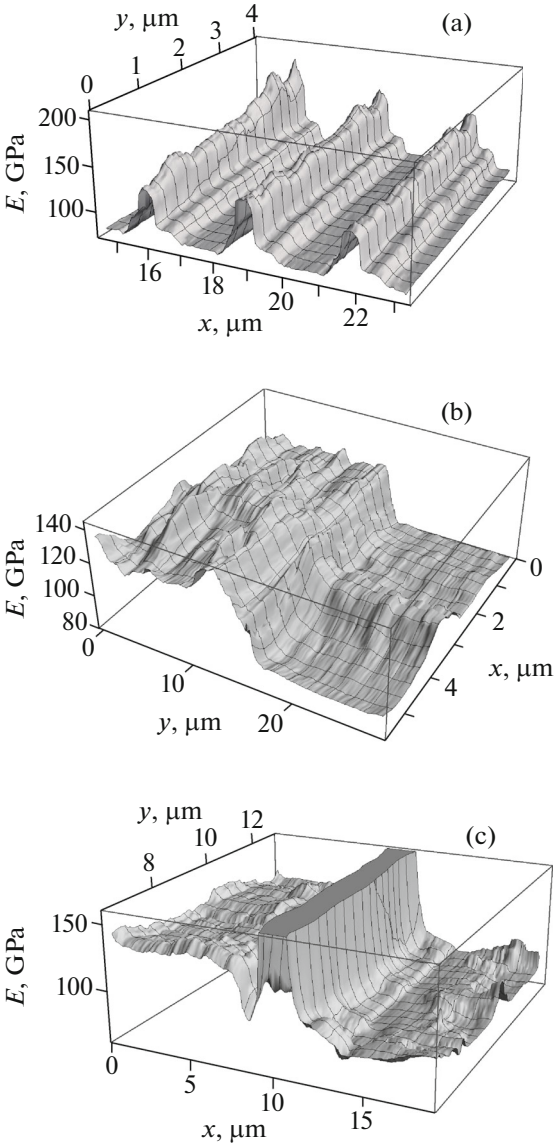

Fig. 3. Elasticity-modulus maps: (a) TGZ test structure; (b) molybdenum films on glass; and (c) copper films on glass.

EXPERIMENTAL VERIFICATION OF THE METHOD

The above-described method was used to process signals that were obtained during scanning of several structures having regions with different mechanical properties.

TGZ-type test structures have been properly studied and are widely used in SPMs [24–26]. They are manufactured via oxidation of the initial silicon substrate and subsequent etching of the oxide layer. As a result, a structure with a known step and a known height is formed, and the silicon-oxide layer thickness of the grating, which was used in the experiment, was 102 nm. Proceeding from the complete multichannel image consisting of 512 × 152 points, we calculated an elasticity-modulus map whose fragment is shown in Fig. 3a. The calculated elasticity-modulus values were filtered with a median filter with a size of 3 × 3 points. The tip oscillation amplitude during scanning was ~4–8 nm, the average pressing force was 10–16 μN, and the operating resonance-frequency shift during scanning was 60 Hz. A spatial resolution of 0.2 μm was attained. The obtained data properly correlate with the elasticity-modulus values for silicon and its oxide.

Metals that are deposited onto solid substrates often serve as objects of nanostructural investigations. An example of mapping mechanical properties of a thin molybdenum layer on glass is shown in Fig. 3b. The coating thickness is 96 nm. The number of processed points is 256 × 50. The obtained elasticity-

modulus values were filtered with a median filter with a size of 5 × 5 points. The probe oscillation amplitude during scanning was ~5–8 nm, the average pressing force was ~6–17 μN, and the operating resonance-frequency shift during scanning was ~60 Hz. The obtained data coincide with the elasticity-modulus values for molybdenum and cover glass.

Thus, the obtained data demonstrate the possibility of quantitative measurements of the elasticity moduli of thin coatings and heterogeneous materials during scanning.

A copper film on glass was also studied. The coating thickness was 410 nm. The number of processed points was 256 × 91. The obtained elasticity-modulus values were filtered with a median filter with a size of 5 × 5 points. The result is shown in Fig. 3c. The probe oscillation amplitude during scanning was ~3.5–8 nm, the average pressing force was ~6–18 μN, and the operating resonance-frequency shift during scanning was ~60 Hz. The image in Fig. 3c has a specific feature—an apparent increase in the elasticity modulus in the transition region between the copper layer and glass. Such a distortion in the actual map of the mechanical properties may be due to a substantial change in the geometry of the contact region: the height difference was rather large (0.415 μm), and a situation becomes possible in which a face of the pyramid but not its tip is in contact with the surface in a given scanned region. Hence, it can be expected that sharp height differences may influence the obtained results when scanning with indenters with large vertex angles.

CONCLUSIONS

The data obtained in this study show the possibility of quantitative mapping of the elasticity modulus of nanostructured materials directly during the scanning procedure. The experimentally attained spatial resolution was 0.2 μm. The proposed theoretical model and the algorithm for processing data on the frequency shift, the amplitude, and the average pressing force of the probe tip applied to the surface were found to be serviceable.

The obtained results indicate the necessity of developing new-generation probes for NanoScan instruments, which must combine high values of the dynamic rigidity of the tuning-fork branches and low values of the static rigidity of the tuning-fork leg. In this case, the required force of pressing the probe tip to the surface of a material can be considerably reduced and soft polymer materials will be available for mapping their elasticity moduli during scanning. At present, when piezoresonance probes are used, which are standard elements for NanoScan instruments, materials with hardnesses of >1 GPa and elasticity moduli of >50 GPa are successfully mapped. When operating with softer materials at pressing forces that are necessary for obtaining a required signal-to-noise ratio, a plastic deformation of the material surface layer is observed in measuring channels, and data on the elasticity-modulus value become distorted.

The proposed approach can be used in both conventional SPMs and nanohardness testers, which are equipped with the in situ surface scanning function and the possibility of monitoring the pressing force, the indenter oscillation amplitude, and the contact rigidity in the region of interaction between the tip and surface.

ACKNOWLEDGMENTS

We are grateful to Dr. Sci. (Phys.–Math.) B.P. Sorokin for granted samples of molybdenum and copper films.

This study was supported by the Ministry of Education and Science of the Russian Federation within the framework of agreement no. 14.577.21.0088 (unique identifier of the RFMEFI57714X0088 project).

REFERENCES

1. Kim, J., Wang, J., Kang, H., and Talke, F., *Polym. Eng. Sci.,* 2008, vol. 48, pp. 277—282. DOI: doi 10.1002/pen.20883
2. Sweers, K., van der Werf, K., Bennink, M., and Subramaniam, V., *Nanoscale Res. Lett.,* 2011, vol. 6, no. 1, p. 270. DOI: 10.1186/1556-276X-6-27010.1186 /1556-276X-6-270
3. Cuy, J.L., Livi, K.J., Teaford, M.F., and Weihs, T.P., *Arch. Oral Biol.,* 2002, vol. 47, pp. 281—1. DOI: 10.1016/ S0003-9969(02)00006-7
4. Franze, K., Francke, M., Gunter, K., Christ, and F., Korber, N., Reichenbach, A., and Guck, J., *Soft Matter.,* 2011, vol. 7, pp. 3147–3154. DOI: 10.1039/C0SM01017K
5. Oliver, W.C. and Pharr, G.M., *J. Mater. Res.,* 2004, vol. 19, pp. 3–20. DOI:10.1557/jmr.2004.19.1.3
6. Maslenikov, I.I., Reshetov, V.N., Loginov, B.A., and Useinov, A.S., *Instrum. Exp. Tech.,* 2015, no. 3 (in press).
7. Syed, A.S.A., Wahl, K.J., Colton, R.J., and Warren, O.L., *J. Appl. Phys.,* 2001, vol. 90, pp. 1192–1200. DOI: 10.1063/1.1380218
8. Magonov, S., *Expanding Atomic Force Microscopy with Hybrid Mode Imaging,* Appl. Note 087. NT-MDT, 2013.
9. Sahin, O. and Erina, N., *Nanotechnology,* 2008, vol. 19, p. 445717. DOI: 10.1088/0957-4484/19/44/445717
10. Schön, P., Bagdi, K., Molnár, K., Markus, P., Pukánszky, B., and Vancso,G.J., *Eur. Polym. J.,* 2011, vol. 47, pp. 692–698. DOI: 10.1016/j.eurpolymj.2010.09.029
11. Dokukin, M.E. and Sokolov, I., *Langmuir,* 2012, vol. 28, pp. 16060–16071. DOI: 10.1021/la302706b
12. Useinov, A., Gogolinskiy, K., and Reshetov, V., *Int. J. Mater. Res.,* 2009, vol. 100, pp. 968–972. DOI: 10.3139/146.110138

13. Soshnikov, A.I., Kravchuk, K.S., Maslenikov, I., Ovchinnikov, D.V., and Reshetov, V.N., *Instrum. Exp. Tech.,* 2013, vol. 56, pp. 133–139. DOI: 10.7868//S0032816213020146
14. Useinov, A.S., Kravchuk, K.S., and Maslenikov, I.I., *Nanoindustriya,* 2013, no. 7, pp. 48–57.
15. Useinov, A.S. and Useinov, S.S., *Philos. Mag.,* 2012, vol. 92, pp. 3188–3198. DOI: 10.1080/14786435.2012.670285
16. Giessibl, F., *Phys. Rev., B: Condens. Matter Mater. Phys.,* 1997, vol. 56, pp. 16010–16015. DOI: 10.1103/PhysRevB.56.16010
17. Durig, U., *Appl. Phys. Lett.,* 1999, vol. 433, pp. 433–435. DOI: doi 10.1063/1.124399
18. Johnson, K., *Contact Mechanics,* Cambridge: University Press, 1987.
19. Fischer-Cripps, A.C., *Nanoindentation*, New York: Springer-Verlag, 2011.
20. Shimamoto, A., Tanaka, K., Akiyma, Y., and Yoshizaki, H., *Philos. Mag. A,* 1996, vol. 74, pp. 1097–1105. DOI: 10.1080/01418619608239710
21. Sawa, T., Akiyama, Y., Shimamoto, A., and Tanaka, K., *J. Mater. Res.,* 1999, vol. 14, pp. 2228–2232. DOI: 10.1557/JMR.1999.0299
22. Sneddon, I., *Int. J. Eng. Sci.,* 1965, vol. 3, pp. 47–57. DOI: 10.1016/0020-7225(65)90019-4
23. Pharr, G.M., Oliver, W.C., and Brotzen, F.R., *J. Mater. Res.,* 1992, vol. 7, pp. 613–617. DOI: doi 10.1557/JMR.1992.0613
24. Korol'kov, V.P. and Konchenko, S.A., *Optoelectron., Instrum. Data Proces.,* 2012, vol. 48, pp. 211–217. DOI: 10.3103/S875669901202015X
25. Gogolinskii, K.V., Gubskii, K.L., Kuznetsov, A.P., Reshetov, V.N., Maslenikov, I.I., Golubev, S.S., Lysenko, V.G., and Rumyantsev, S.I., *Measur. Tech.,* 2012, vol. 55, pp. 400–405. DOI: 10.1007/s11018-012-9972-4
26. http://www.spmtips.com/test-structures-TGXYZ-series.html [Online]

Translated by A. Seferov